TÜBİTAK

Turkish Journal of Physics

http://journals.tubitak.gov.tr/physics/

Research Article

Turk J Phys
(2018) 42: 356 – 367

doi:10.3906/fiz-1801-34

Analysis of quantum-dot-embedded multicavity arrays for on-chip WDM applications

Havva ERDİNÇ, Serdar KOCAMAN*
Department of Electrical and Electronics Engineering, Faculty of Engineering, Middle East Technical University, Ankara, Turkey

Received: 30.01.2018 • **Accepted/Published Online:** 09.07.2018 • **Final Version:** 15.08.2018

Abstract: Transmission and group delay characteristics of a single-quantum-dot-(QD)-embedded double-cavity array and a triple-cavity array are compared theoretically in the weak coupling regime. When the extrinsic cavity decay rate is comparably higher than the intrinsic cavity decay rate at equal coupling strengths and normalized detuning values, transmission values of both systems converge with each other but the phase delay generated at triple-cavity systems is higher than that of the single-QD-embedded double-cavity array system. The results confirmed by the transmission calculations for both cases provide a comparative tool for designing onchip wavelength division multiplexing systems.

Key words: Quantum dot, cavity quantum electrodynamics, on-chip wavelength division multiplexing, long-distance quantum communication

1. Introduction

Recently, semiconductor technologies based on cavity quantum electrodynamics (CQED) have made a huge progress because of the optical microcavities with high quality factors and less than a cubic wavelength mode volumes [1–3]. In these microresonators, light is confined to small volumes with the help of resonant recirculation and behaves differently compared to free space travel leading to many application fields such as narrow spot-size laser read/write beams, emission of spontaneous photons in a desired direction, and long-distance communication [4–5]. For instance, quantum information processing can provide secure data transmission between distances as long as a thousand kilometers [6–8], which makes quantum communication a frequently preferred technology for long-distance high-security links. With the help of the strong interaction between light and matter, quantum information science involves storage, manipulation, and transfer of information encoded in quantum systems, where the phenomena of superposition and entanglement provide enhancements over what was classically possible [9–12].

Wavelength division multiplexing (WDM) has been a popular method with increased data transmission demand globally. In this method, only a single optical link can transfer multiple data streams with the possibility of adding/subtracting data channels at various locations [13]. As a result, a huge bandwidth, low signal attenuation, low distortion, low power requirement, and low cost can be obtained [14]. Increasing the network capacity without installing new fiber optical links is an important advantage for telecommunication companies [13,15]. The WDM technology is categorized as bidirectional wave division multiplexing (BWDM), coarse wave

*Correspondence: skocaman@metu.edu.tr

division multiplexing (CWDM), and dense wave division multiplexing (DWDM) [16], among which DWDM has the maximum capacity for the number of channels. In addition, mode-division multiplexing (MDM), in conjunction with WDM, has also been studied in order to further increase the bandwidth [17,18].

In the present study, phase delay generation via CQED for WDM channels was simultaneously analyzed in order to support the effort toward higher performance systems. Depending on the lifetime characteristics of the microcavities, higher propagation delay can be obtained either with systems consisting solely of microcavities or with systems including cavities coupled with QDs. For the sake of concept demonstration, two-channel systems have been utilized here. However, the number of the microresonators can be increased to enlarge the number of channels in the transmission links.

2. Theoretical model

Optical analogue of electromagnetically induced transparency (EIT) is one of the prominent methods in obtaining propagation delay in integrated optical systems [19,20]. In the systems involving both photonic crystal cavities and QDs, if the coupling strength (g) is much smaller than the cavity decay rate (2Γ), the QDs and cavities are weakly coupled whereas there is a strong coupling in the opposite case ($2\Gamma << g$) [21,22]. Strong coupling has many applications such as conditional phase shifts on single photons and atom number detection [1,2]. However, for the chip-scale applications, cavity-waveguide coupling makes the strong coupling difficult and, therefore, weak coupling is preferred [1,20]. In this regard, high-Q double-cavity array and QD-embedded single-cavity systems in the weak coupling regime systems are compared recently and the generated delay was twice as high for the multicavity case [20]. In our study, single-QD-embedded double-cavity array and triple-cavity array systems are modeled with the same formalism and the spectral characteristics in terms of transmission, and the generated group delays are compared. Initially, one cavity interacting with a QD (Figure 1) subsystem is examined, and then the formulation is generalized for these systems.

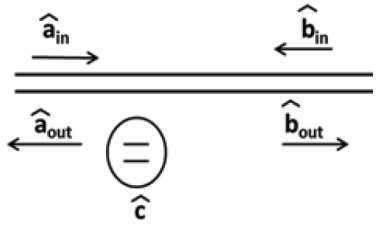

Figure 1. Schematic for the cavity QD system.

Heisenberg equations of motion are obtained easily [9]:

$$\frac{d\hat{c}}{dt} = -i\left[\hat{c}, \mathrm{H}\right] - \Gamma\hat{c} + \sqrt{\kappa_1}\left(\hat{a}_{in} + \hat{b}_{in}\right) \tag{1}$$

$$\frac{d\hat{\sigma}_-}{dt} = -i\left[\hat{\sigma}_-, \mathrm{H}\right] - \gamma\hat{\sigma}_- + \sqrt{\dot{\gamma}}\dot{\hat{\sigma}}' \tag{2}$$

In this formula, $\hat{c}$ is the basonic annihilation operator of the cavity mode with resonant frequency $\omega_{\mathbf{c}}$. The input and output fields of the QD system with extrinsic cavity decay rate ($\kappa_{\mathbf{1}}$) is written as follows [20,23]:

$$\hat{a}_{out} = \hat{b}_{in} - \sqrt{\kappa_1}\hat{c} \tag{3}$$

$$\hat{b}_{out} = \hat{a}_{in} - \sqrt{\kappa_1}\hat{c} \tag{4}$$

In Heisenberg equations, $\mathbf{2\Gamma}$ defines the total cavity decay rate ($\Gamma = (\kappa_0 + \mathbf{2}\kappa_1)/\mathbf{2}$), where κ_0 is the intrinsic cavity decay rate, $\hat{\sigma}_-$ is the descending operator of the interacting two-level QD with transition frequency ω_r, $\dot{\hat{\sigma}}'$ is the vacuum noise operator related to the γ total decay rate, and H is the Hamiltonian operator which consists of $\mathbf{g}$ (coupling strength between the cavity mode and the dipolar transition between the excited and ground states of the QD), ω_c (cavity mode resonant frequency), and ω_r (QD transition frequency) [23]:

$$\mathbf{H} = \omega_c \hat{c}^{\dagger}\hat{c} + \omega_r \hat{\sigma}_- + [\mathbf{g}\hat{\sigma}_- \hat{c} + \mathbf{h.c}] \tag{5}$$

If the motion equations are solved in the weak excitation limits, the transport relations in the frequency domain becomes as follows [20,23]:

$$\begin{pmatrix} \hat{b}_{in}(\omega) \\ \hat{b}_{out}(\omega) \end{pmatrix} = \frac{1}{\alpha - \Gamma + \kappa_1} \begin{pmatrix} -\kappa_1 & \alpha - \Gamma \\ \alpha - \Gamma + 2\kappa_1 & -\kappa_1 \end{pmatrix} \begin{pmatrix} \hat{a}_{in}(\omega) \\ \hat{a}_{out}(\omega) \end{pmatrix} \tag{6}$$

where $\alpha = \mathbf{i}(\omega - \omega_c) + \frac{|\mathbf{g}|^2}{\mathbf{i}(\omega - \omega_r) - \gamma}$

This definition presents the single-cavity-QD system shown in Figure 1. In case the QD is on-resonant with the cavity mode, the transition frequency of the QD is equal to the cavity resonant frequency. The coupling strength (g) between the cavity mode and the QD transition manipulates the splitting of the transmitted field [1]. The transmission spectrum for this system is shown in Figure 2, where there is a transparency window with an associated propagation delay at the resonant frequency [20].

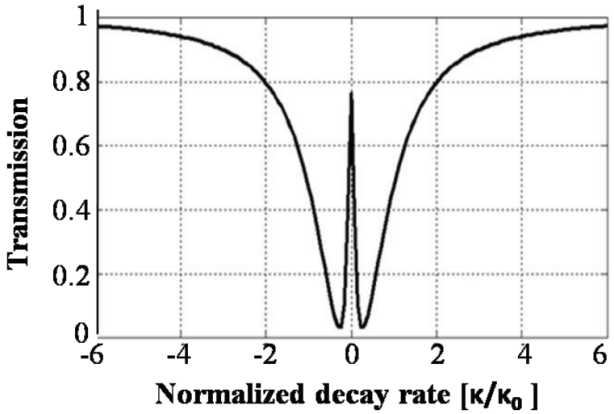

Figure 2. Schematic for the cavity QD EIT (classical EIT).

As the purpose here is to generalize this concept for multichannel systems to be utilized in the WDM applications, there is a need for multiple transparency windows. For instance, two channels can be achieved with either three cavities [24,25] or two cavities one of which has an embedded QD in it [23]. Even though various configurations were proposed before, alternative systems that can provide multiple channels have not been comparatively analyzed yet.

Next, two of these systems shown in Figures 3a and 3b are modeled with the same formalism.

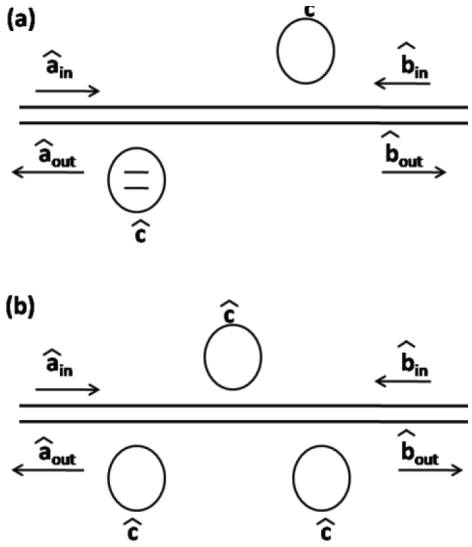

Figure 3. Schematic for the single-QD double-cavity array (a) and the triple-cavity array (b).

Equations for the double-cavity array with QD are derived by cascading two single cavities with a QD together with a phase component for the coupling waveguide. For the second cavity, the coupling strength between the QD and the cavity has been set to zero leading to the system described in Figure 3a. The resulting transport relation for this system is shown in Eq. (7):

$$\begin{pmatrix} \hat{b}_{\mathbf{in}}(\omega) \\ \hat{b}_{\mathbf{out}}(\omega) \end{pmatrix} = \frac{\mathbf{1}}{\beta-\Gamma_{\mathbf{2}}+\kappa_{\mathbf{2}}} \begin{pmatrix} -\kappa_{\mathbf{2}} & \beta-\Gamma_{\mathbf{2}} \\ \beta-\Gamma_{\mathbf{2}}+\mathbf{2}\kappa_{\mathbf{2}} & \kappa_{\mathbf{2}} \end{pmatrix} \begin{pmatrix} \mathbf{0} & \mathbf{e}^{\mathbf{j}2\pi} \\ \mathbf{e}^{\mathbf{j}2\pi} & \mathbf{0} \end{pmatrix}$$

$$\frac{\mathbf{1}}{\alpha-\Gamma_{\mathbf{1}}+\kappa_{\mathbf{1}}} \begin{pmatrix} -\kappa_{\mathbf{1}} & \alpha-\Gamma_{\mathbf{1}} \\ \alpha-\Gamma_{\mathbf{1}}+\mathbf{2}\kappa_{\mathbf{1}} & \kappa_{\mathbf{1}} \end{pmatrix} \begin{pmatrix} \hat{a}_{\mathbf{in}}(\omega) \\ \hat{a}_{\mathbf{out}}(\omega) \end{pmatrix} \tag{7}$$

where

$$\alpha = \mathbf{i}(\omega-\omega_{\mathbf{c1}}) + \frac{|\mathbf{g}|^{\mathbf{2}}}{\mathbf{i}(\omega-\omega_{\mathbf{r}})-\gamma}$$

and $\beta = \mathbf{i}(\omega-\omega_{\mathbf{c2}})$.

Furthermore, in order to obtain the same relation for the triple-cavity system shown in Figure 3b, three of the single-cavity systems have been cascaded again by setting the coupling strengths to zero. Eq. (8) shows the transport matrix components:

$$\begin{pmatrix} \hat{b}_{\mathbf{in}}(\omega) \\ \hat{b}_{\mathbf{out}}(\omega) \end{pmatrix} = \frac{\mathbf{1}}{\beta_{\mathbf{3}}-\Gamma_{\mathbf{3}}+\kappa_{\mathbf{3}}} \begin{pmatrix} -\kappa_{\mathbf{3}} & \beta_{\mathbf{3}}-\Gamma_{\mathbf{3}} \\ \beta_{\mathbf{3}}-\Gamma_{\mathbf{3}}+\mathbf{2}\kappa_{\mathbf{3}} & \kappa_{\mathbf{3}} \end{pmatrix} \begin{pmatrix} \mathbf{0} & \mathbf{e}^{\mathbf{j}2\pi} \\ \mathbf{e}^{\mathbf{j}2\pi} & \mathbf{0} \end{pmatrix}$$

$$\frac{\mathbf{1}}{\beta_{\mathbf{2}}-\Gamma_{\mathbf{2}}+\kappa_{\mathbf{2}}} \begin{pmatrix} -\kappa_{\mathbf{2}} & \beta_{\mathbf{2}}-\Gamma_{\mathbf{2}} \\ \beta_{\mathbf{2}}-\Gamma_{\mathbf{2}}+\mathbf{2}\kappa_{\mathbf{2}} & \kappa_{\mathbf{2}} \end{pmatrix} \begin{pmatrix} \mathbf{0} & \mathbf{e}^{\mathbf{j}2\pi} \\ \mathbf{e}^{\mathbf{j}2\pi} & \mathbf{0} \end{pmatrix}$$

$$\frac{\mathbf{1}}{\beta_{\mathbf{1}}-\Gamma_{\mathbf{1}}+\kappa_{\mathbf{1}}}\begin{pmatrix} -\kappa_{\mathbf{1}} & \beta_{\mathbf{1}}-\Gamma_{\mathbf{1}} \\ \beta_{\mathbf{1}}-\Gamma_{\mathbf{1}}+\mathbf{2}\kappa_{\mathbf{1}} & \kappa_{\mathbf{1}} \end{pmatrix}\begin{pmatrix} \hat{a}_{\mathbf{in}}(\omega) \\ \hat{a}_{\mathbf{out}}(\omega) \end{pmatrix} \tag{8}$$

where $\beta_{\mathbf{j}}=\mathbf{i}(\omega-\omega_{\mathbf{j}})$.

The spectral characteristics should be analyzed in order to model the physical behavior of these systems. The transmission and reflection values can be calculated by solving Eqs. (7) and (8) and $\mathbf{t}=\hat{a}_{\mathbf{out}}\big/\hat{b}_{\mathbf{in}}$ and $\mathbf{r}=\hat{b}_{\mathbf{out}}\big/\hat{a}_{\mathbf{in}}$ are obtained, respectively. In addition, the phase of the transmitted field can be defined as $\phi=\angle(\hat{b}_{\mathbf{out}}\big/\hat{a}_{\mathbf{in}})$ [20,23].

In order to get the spectral characteristics, these equations have been solved for a variety of frequency values, and the comparison results in terms of the transmission spectra, phase of the transmitted fields, and group delay ($\mathbf{d}\phi/\mathbf{d}\omega$) values are summarized in Figure 4 for both double-cavity with a QD and triple-cavity systems.

Figure 4a shows the spectral transmission characteristics for the case where a single QD is embedded in a double-cavity array where the QD resonantly interacts with the first cavity. The value of the intrinsic and extrinsic cavity decay rates is the same for both cavities, and the QD transition (ω_r) and cavity resonant frequencies (ω_c) are equal. Transmission values at both channels are the same as expected as the system is on-resonant ($\omega_r=\omega_c$). Figure 4b summarizes the group delay generated where both channels have again the same value. In terms of the tuning capability, if the coupling strength that is responsible for the splitting is changed, the center frequency of the channels in the WDM system can be adjusted. For example, the transmission spectra where the difference between the resonance frequencies are set to 0.5Γ, 1.33Γ and 5Γ are shown with red, black and blue lines, respectively in Figure 4c.

Moreover, Figure 4d shows the spectral transmission characteristics of the triple-cavity case where decay rates are all identical for the cavities and the resonant frequencies are modified for the first and third cavity (-$\Delta\omega$, 0, $\Delta\omega$) so that a symmetric transmission spectrum is obtained in the normalized frequency dimensions. As mentioned above, the coupling strength value is assumed to be zero because there are no QDs in the cavities. Furthermore, the optical path between the cavities has been set not to introduce any additional phase accumulation as the coherent interaction occurs if and only if the bus waveguide has an integer multiple of 2π [24, 25]. The group delays corresponding to the calculated transmission spectrum are given in Figure 4e. Similar to the previous case, both channels have the same transmission and group delay characteristics. Then, the same variation as in Figure 4c is applied to triple-cavity case in order to demonstrate the tuning and the results are summarized in Figure 4f. As a result, the transmission characteristics (Figures 4a and 4d) and the corresponding phase/group delay values (Figures 4b and 4e) together with the tuning characteristics (Figures 4c and 4f) look similar for both systems showing that these two systems can indeed be interchangeable and detailed comparison for a potential WDM application is useful.

3. Transmission and group delay comparison

Next, the transmission and group delay characteristics are analytically compared for both configurations. In order to get a simpler formalism, cavity decay rates are assumed to have the same values ($\kappa_{\mathbf{3}}=\kappa_{\mathbf{2}}=\kappa_{\mathbf{1}}=\kappa$ and $\Gamma_{\mathbf{3}}=\Gamma_{\mathbf{2}}=\Gamma_{\mathbf{1}}=\Gamma$).

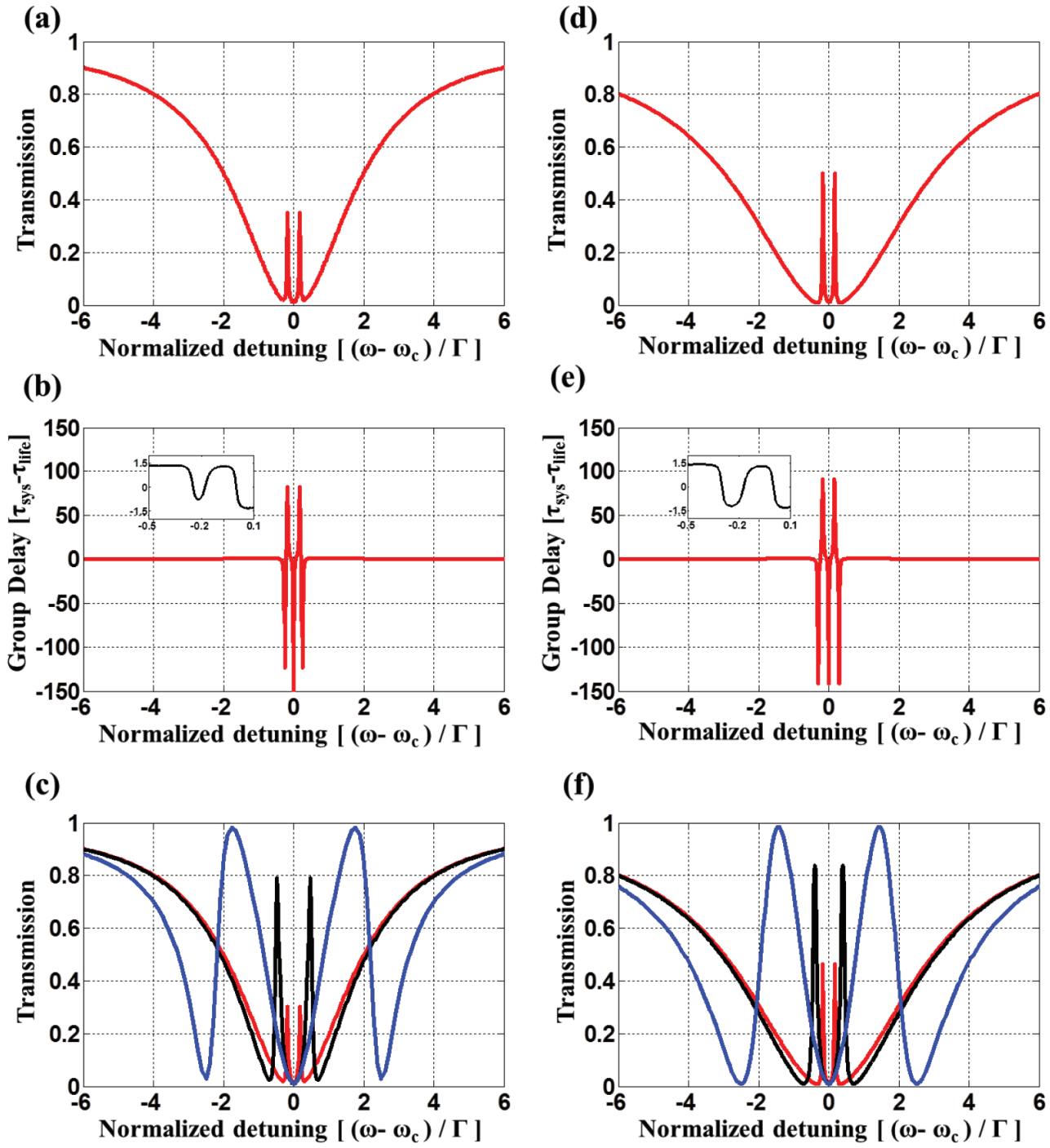

Figure 4. The transmission spectrum for the single-QD-embedded double-cavity array (a) and the triple-cavity array (b). Phase and group delay (c) and (d), respectively corresponding to (a) and (b). Transmission variation with various detuning for single-QD-embedded double-cavity array (e) and the triple-cavity array (f).

Eqs. (7) and (8) are solved for $\hat{a}_{\mathbf{out}}\Big/\hat{b}_{\mathbf{in}}$ separately and the frequency dependent transmission expressions are obtained:

$$\mathbf{t}(\omega)=\frac{\left(2\omega^2\kappa_0-\frac{1}{2}g^2\kappa_0-\frac{1}{4}\kappa_0^3\right)+i\omega\left(-\omega^2+g^2+\frac{5}{4}\kappa_0^2\right)}{\left(2\omega^2\kappa_0+2\kappa\omega^2-\kappa g^2-\frac{1}{2}g^2\kappa_0-\kappa\kappa_0^2-\frac{1}{4}\kappa_0^3\right)+i\omega\left(g^2-\omega^2+3\kappa\kappa_0+\frac{5}{4}\kappa_0^2\right)} \tag{9}$$

$$\mathbf{t}(\omega)=\frac{\left(2\omega^2\kappa_0-\frac{1}{2}g^2\kappa_0\right)+i\omega\left(-\omega^2+g^2\right)}{\left(2\omega^2\kappa-\kappa g^2-\kappa\kappa_0^2\right)+i\omega\left(-\omega^2+g^2+3\kappa\kappa_0\right)} \tag{10}$$

These equations can be simplified considering the physical characteristics of the systems analyzed here. In particular, the extrinsic cavity decay rate is usually much greater than the intrinsic cavity decay rate ($\kappa >> \kappa_0$) for the on-chip applications in order to maintain the connection with the rest of the network through the coupling waveguide. If this condition is applied to Eqs. (9) and (10), simpler transmission expressions, Eqs (11) and (A.1), are obtained for the QD-embedded double-cavity and the triple-cavity cases, respectively. Then, the systems analyzed above are compared while the various parameters are tuned.

$$\mathbf{t}(\omega)=\frac{\left(\frac{3}{2}\omega^2\kappa_0-\frac{1}{2}\kappa_0\,\omega^2\right)+i\omega\left(-\omega^2+\omega^2\right)}{\left(3\omega^2\kappa-\omega^2\kappa-\frac{3}{4}\kappa\kappa_0^2\right)+i\omega\left(-\omega^2+\omega^2+3\kappa\kappa_0\right)} \tag{11}$$

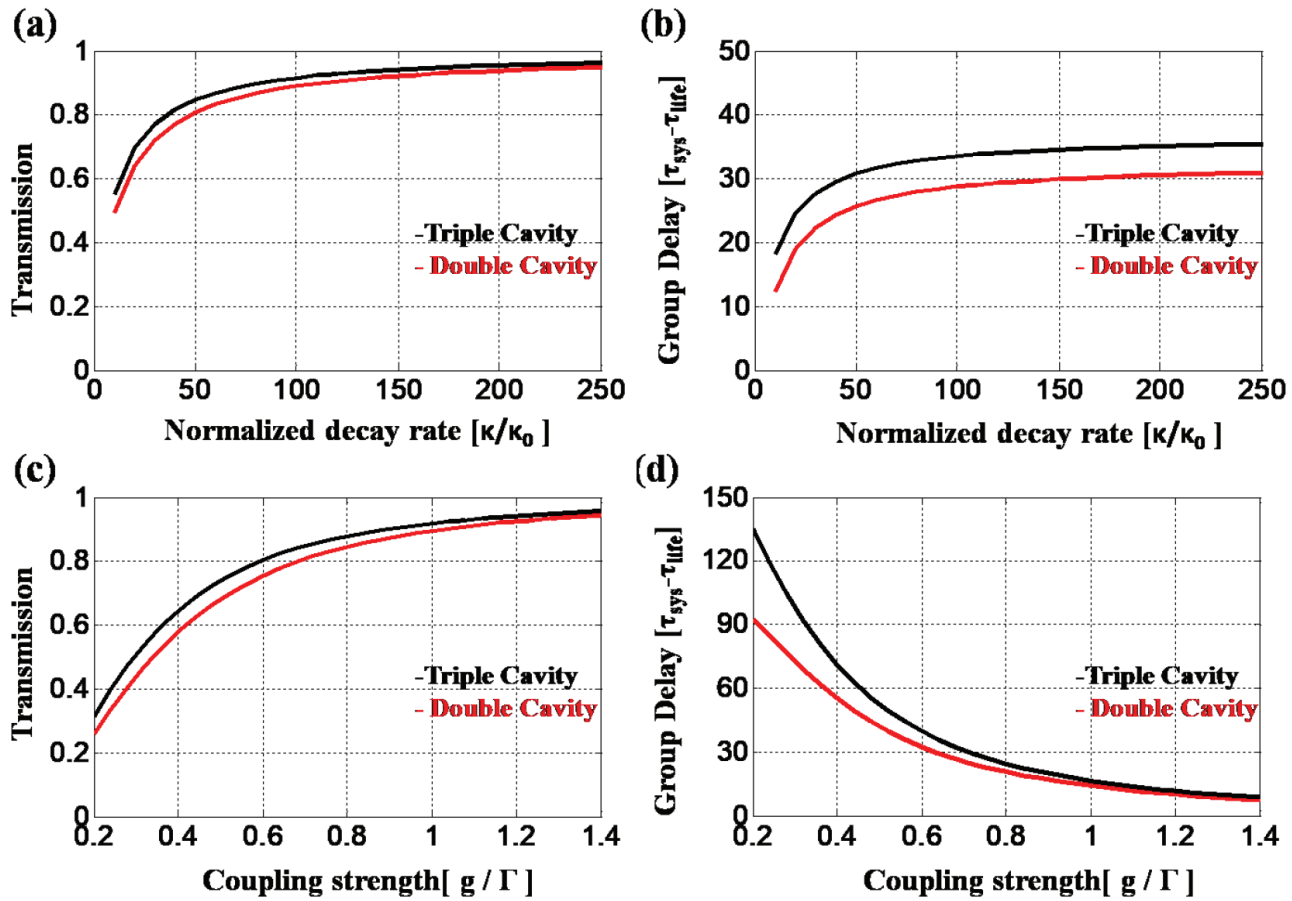

Figure 5. Comparison of the transmission spectrum (a) and generated group delay (b) of the single-QD-embedded double-cavity array and the triple-cavity array with the coupling strength of 0.7?. Transmission (c) and group delay (d) graphs are repeated for the coupling strength scan with $\kappa = 5\kappa_0$.

$$\mathbf{t}(\omega)=\frac{\left(\frac{\mathbf{3}}{\mathbf{2}}\omega^{\mathbf{2}}\kappa_{\mathbf{0}}-\frac{\mathbf{1}}{\mathbf{2}}\kappa_{\mathbf{0}}\,\omega^{\mathbf{2}}\right)+\mathbf{i}\omega\left(-\omega^{\mathbf{2}}+\omega^{\mathbf{2}}\right)}{\left(\mathbf{3}\omega^{\mathbf{2}}\kappa-\omega^{\mathbf{2}}\kappa-\frac{\mathbf{3}}{\mathbf{4}}\kappa\kappa_{\mathbf{0}}^{\mathbf{2}}\right)+\mathbf{i}\omega\left(-\omega^{\mathbf{2}}+\omega^{\mathbf{2}}+\mathbf{3}\kappa\kappa_{\mathbf{0}}\right)} \tag{12}$$

Firstly, the extrinsic cavity decay rate value (κ) is changed from $20\kappa_0$ to $250\kappa_0$ with equal steps and the transmission spectra and group delay values are calculated for both configurations. In Figure 5a, where the resonant frequencies are –0.7Γ, 0, and 0.7Γ for the ω_{c1}, ω_{c2}, and ω_{c3} resonant frequencies, respectively and the coupling strength value (g) is set to 0.7Γ, the transmission values of the triple-cavity and the single-QD-embedded double-cavity array systems are interestingly equal especially at high extrinsic cavity decay rates. Concerning the group delay, the results are even more interesting. As can be seen in Figure 5b, the triple-cavity system consistently generates higher group delay values than the QD-embedded double-cavity system.

Then, the frequency detuning dependency of the spectral characteristics has also been analyzed. This detuning corresponds to the frequency spacing between different channels in the WDM systems. Frequency splitting in the transmission spectrum comes from the coupling strength between the QD cavities in the QD-embedded double-cavity system and from the resonant frequency difference in the triple-cavity system. When the coupling strength changes, the normalized detuning values differ at the same rate as in the triple-cavity system.

This tuning has been scanned from 0.2Γ to 1.4Γ while $\kappa = 50\kappa_0$ and the results are summarized in Figures 5c and 5d. The transmission values increase and the generated group delay decreases with increasing frequency detuning as expected due to the fact that the delay bandwidth product is constant unless there is a dynamical tuning [26]. In terms of the propagation delay value, the triple-cavity phase delay values are still higher than those of the single-QD-embedded double-cavity array system.

Next, the calculations in Figure 5 are repeated for a different set of parameters. In particular, the extrinsic cavity decay rate scan has been run with smaller detuning ($g = 0.3\Gamma$ and $\Delta\omega = 0.3\Gamma$) values and the results are shown in Figures 6a and 6b. The observed characteristics above are again present in this case with the fact that the exact values have been changed. The triple-cavity transmission and phase delay values are still higher than those of the single-QD-embedded double-cavity array system. On the other hand, smaller detuning results in higher phase delay values. At a lower rate of extrinsic cavity decay ($\kappa = 10\kappa_0$), the coupling strength scan results in phase delay characteristics where there is an optimum value for the maximum propagation delay as shown in Figures 6c and 6d. This behavior is similar to that of the single-channel case [20].

Up to this point, the transmission values of the single-QD-embedded double-cavity and the triple-cavity are made nearly equal to each other by choosing the same coupling strength and normalized detuning. As a result, the minimum transmission points of both systems were equal but the maximum points were not exactly same. However, considering the WDM applications, maximum transmission values are quite critical as well. Therefore, the simulations have been repeated by manipulating the coupling strength and normalized detuning values to get the maximum transmission value at the same ω point. In particular, the extrinsic cavity decay rate scan has been run with $g = 0.3\Gamma$ and $\Delta\omega = 0.25\Gamma$ and the transmission results are shown in Figure 7a.

Considering the group delay, the results are quite interesting. As can be seen in Figure 7b, the triple-cavity system generates higher group delays than the QD-embedded double-cavity system when the extrinsic cavity decay rate is smaller than $55\kappa_0$. However, over $55\kappa_0$, the triple-cavity group delay is lower than that of the QD-embedded double-cavity system. Therefore, the comparative results in Figure 7b show that the preference in selecting the group delay component during system designs when both configurations are available can be changed with respect to the parameters.

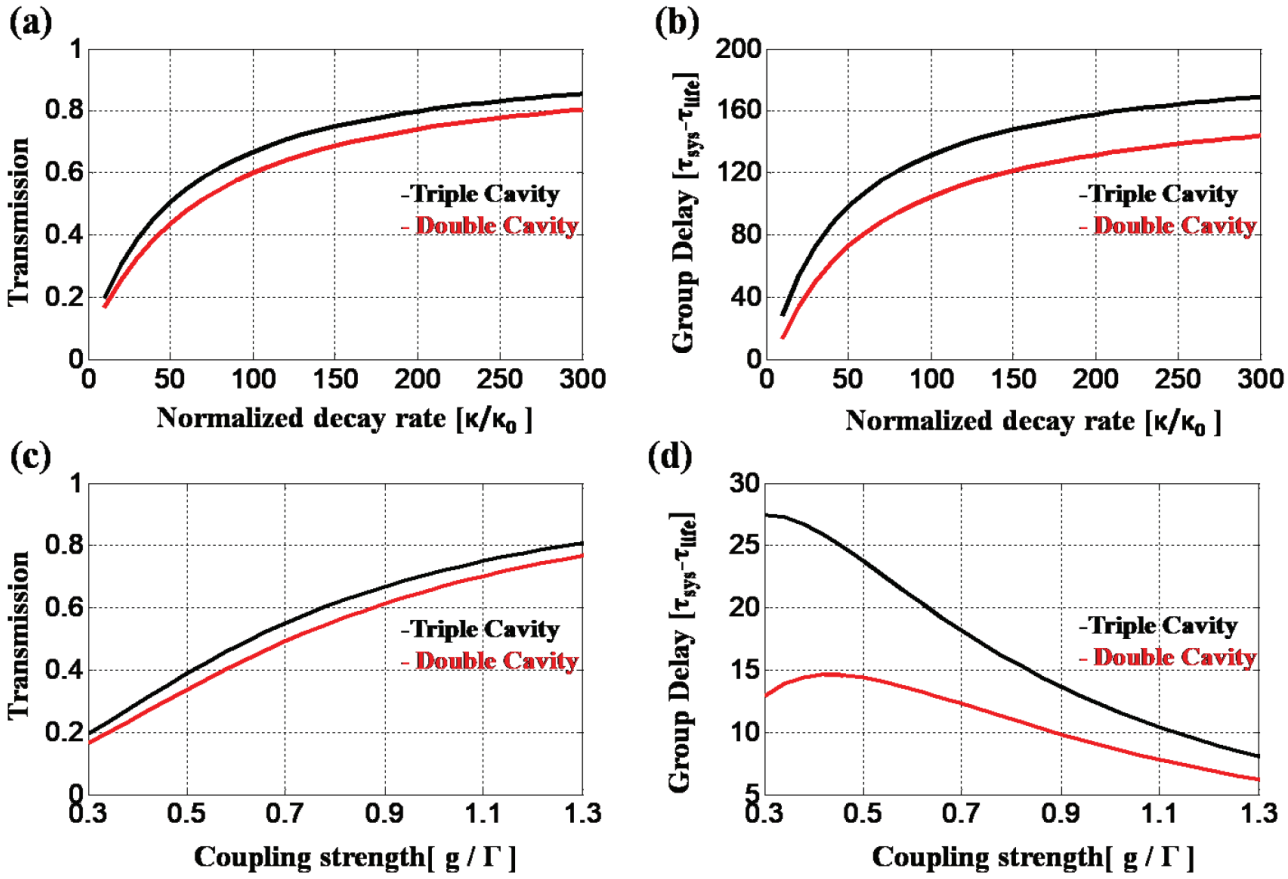

Figure 6. Comparison of the transmission spectrum (a) and generated group delay (b) of the single-QD-embedded double-cavity array and triple cavity array with the coupling strength of 0.3Γ. Transmission (c) and group delay (d) graphs are repeated for the coupling strength scan with $\kappa = \mathbf{10}\kappa_{\mathbf{0}}$.

Then, the frequency detuning dependency of the spectral characteristics have also been analyzed with a coupling strength (g) scan from 0.2Γ to 1.4Γ and the corresponding frequency detuning ($\Delta\omega$). The results are summarized in Figures 7c and 7d. The transmission values increase and the generated group delay again decreases with increasing frequency detuning. In terms of the propagation delay value, there is also an intersection where the generated delay is higher for the triple-cavity case for smaller detuning values and lower for larger detuning values.

As the intersection points in Figures 7b and 7d are quite interesting, further analysis is necessary in order to fully understand this characteristic. The dependency of the intersection points with respect to the coupling strength value and cavity decay rate has been calculated and the results are summarized in Figure 8. The point where the QD-embedded double-cavity system starts having higher propagation delay values with respect to the increasing extrinsic cavity decay rate seems to be getting smaller as the coupling strength (and the corresponding normalized detuning) value increases.

As a result, when the extrinsic cavity decay rate is much higher than the intrinsic cavity decay rate, which is the case for on-chip devices, the transmission characteristics seem to be similar. However, in terms of the generated group delay, the value of the coupling strength is important and depending on the system parameters, the better choice can be different.

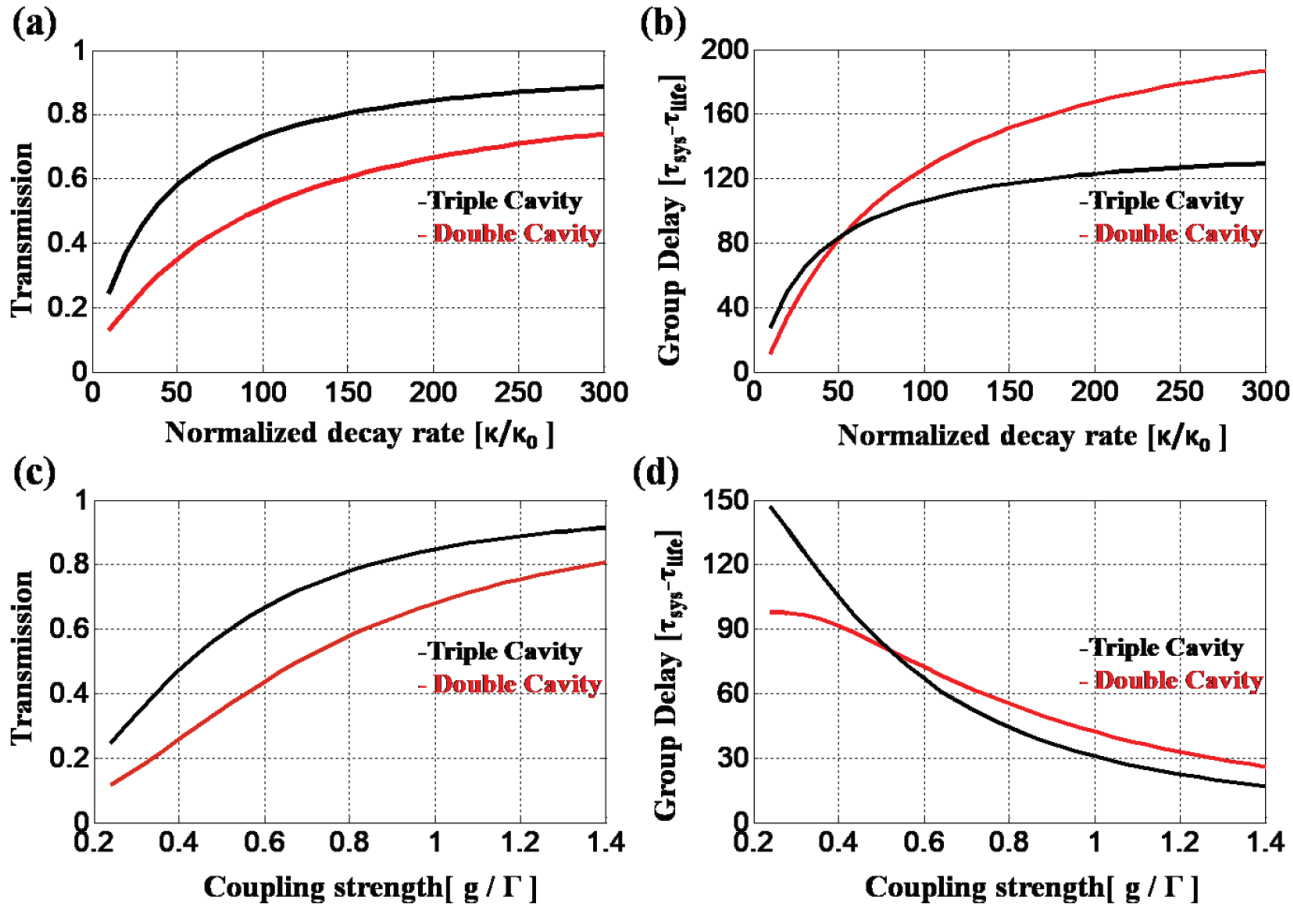

Figure 7. Comparison of the transmission spectrum (a) and generated group delay (b) of the single-QD-embedded double-cavity array and the triple-cavity array with the coupling strength of 0.3Γ. Transmission (c) and group delay (d) graphs are repeated for $\kappa = \mathbf{50}\kappa_{\mathbf{0}}$.

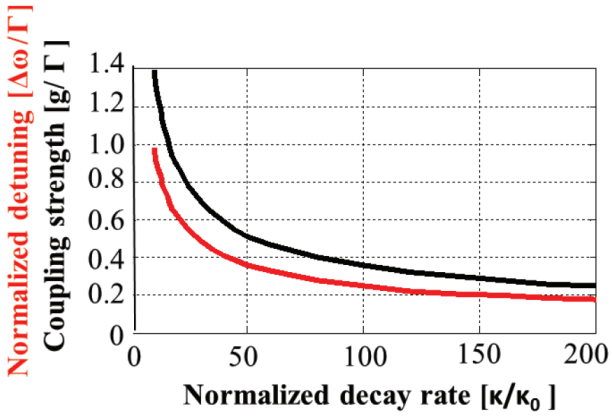

Figure 8. Group delay intersection values for coupling strength and normalized detuning.

4. Conclusion

In summary, single-QD-embedded double-cavity array under weak coupling regime and triple-cavity array systems are compared in terms of the transmission spectrum and generated temporal group delay. Coupling

strength and the cavity decay rate are the two important parameters in this comparison. In particular, the Vacuum Rabi splitting, which determines the spectral difference between the transmission deeps, is controlled by the coupling strength. In addition, quality factors are another measure of the decay rates. As a result, these two parameters are directly responsible for the characteristics of the transmission spectrum. Since the dispersive behavior coming from the optical filter nature of the cavities and the systems discussed here has a limitation on the generated group delay depending on the spectral linewidth, i.e. the delay-bandwidth product, these two parameters effectively determine the delay as well.

As a result, when the extrinsic cavity decay rate is higher than the intrinsic cavity decay rate, the transmission values converge with each other when the coupling strength and the frequency detuning are equal. In addition, the triple-cavity phase delay is higher than that of the single-QD-embedded double-cavity array. Higher extrinsic cavity decay rates and smaller coupling strength values result in higher phase delay values. Furthermore, if the coupling strength values and normalized detuning values are chosen to get the maximum transmission values at the same frequency, transmission values of the triple-cavity are higher than those of the single-QD-embedded double-cavity array and there is an intersection point in terms of the propagation delay where the higher group delay system changes as the coupling strengths and extrinsic cavity decay rates vary. Therefore, both systems can be preferable for supplying group delays for the on-chip WDM applications depending on the component parameters.

References

[1] Waks, E.; Vuckovic, *Phys. Rev. Lett.* **2006**, *96,* 1-4.

[2] Haroche, S. *Conference on Coherence and Qauntum Optics 2007*, Rochester, NY, USA, 10–13 June 2007.

[3] Englund, D.; Fushman, I.; Vucković, J. *Opt. Express.* **2005**, *13*, 61-75.

[4] Morin, S. E.; Wu, Q.; Mossberg. T. W. *Opt. Photonics News* August 1992, pp. 8-15.

[5] Vahala, K. J. *Nature* **2004**, *424*, 839-846.

[6] Duan, L. M.; Lukin, M.; Cirac, I.; Zoller, P. *Nature* **2001**, *414*, 413-418.

[7] Chou, C. W.; Polyakov, S. V.; Felinto, D.; De Riedmatten, H.; Van Enk S. J.; Kimble, H. J. In Quantum Information with Continuous Variables of Atoms and Light; Cerf, N. J.; Leuchs, N.; Polzik, E. S., Eds. Imperial College Press: London, UK, 2007, pp. 553-580.

[8] Muralidharan, S.; Li, K.; Lütkenhaus, N; Lukin, M. D.; Jiang L. *Sci. Rep-UK* **2016**, *6*, 20463-20473.

[9] Wallraf, A.; Schuster, D. I.; Blais, A.; Frunzio, L.; Huang, R.S.; Majer, J.; Kumar, S.; Girvin, S. M.; Schoelkopf, R. J. *Nature* **2004**, *431*, 162-167.

[10] Vuckovic, J.; Englund, D.; Faraon, A.; Fushman, I.; Waks, E. In *Semiconductor Quantum Bits*; Benson O.; Henneberger F., Eds. Pan Stanford Publishing: Singapore, 2008, pp. 423-452.

[11] Moehring, D. L.; Maunz, P.; Olmschenk, S.; Younge, K. C.; Matsukevich, D. N.; Duan, L.M.; Monroe, C. *Nature* **2007**, *449*, 68-71.

[12] Spiller T. P. *Mater. Today* **2003**, *6*, 30-36.

[13] Sletteng, B. R.; Asa, N. E. *Int. J. Eng. Sci.* **2002**, *4*, 1-4.

[14] Mukherjee, B. *IEEE J. Sel. Area. Com.* **2000**, *18*, 1810-1824.

[15] Müstecaplioglu Ö. E. *Opt. Photonics News* **2008**, *19*, 26-31.

[16] Bhatt, S.; Jhaveri, S. *International Journal of Innovative Science, Engineering and Technology* **2013**, *2*, 404-412.

[17] Luo, L. W.; Ophir N.; Chen, C. P.; Gabrielli, L. H.; Poitras, C. B.; Bergmen, K.; Lipson, M. *Nat. Commun.* **2014**, *5*, 1-7.

[18] Ye, M.; Yu, Y.; Luo, Y.; Zhang, X. *Opt. Express* **2015**, *23*, 32130-32138.

[19] Harris, S. E. *Phys. Today* **1997**, *50*, 36-42.

[20] Kocaman, S.; Turhan Sayan, G. *Opt. Express* **2016**, *24*, 29329-29341.

[21] Majumdar A. PhD, Department of Electrical Engineering, Stanford University, Stanford, CA, USA, 2012.

[22] Fushman, I. PhD, Department of Applied Physics, Stanford University, Stanford, CA, USA, 2008.

[23] Xiao, Y. F.; Gao, J.; Zou, X. B.; McMillan, J. F.; Yang, X.; Chen, Y. *New J. Phys.* **2008**, *10*,123013-123026.

[24] Kocaman, S.; Yang, X.; McMillan, J. F.; Yu, M. B.; Kwong, D. L.; Wong, W. *Appl. Phys. Lett.* **2010**, *96*, 221111-221114.

[25] Gu, T.; Kocaman, S.; Yang, X.; McMillan, J. F. ; Yu, M.; Lo,G. Q.; Kwong, D. L.; Wong, C. W. *Appl. Phys. Lett.* **2011**, *98*, 121103-121109.

[26] Xu, Q.; Dong, P.; Lipson, M. *Nat. Phys.* **2007**, *3*, 406-410.

Appendix

$\kappa_{\mathbf{1}}$: extrinsic cavity decay rate

$\kappa_{\mathbf{0}}$: intrinsic cavity decay rate

$\mathbf{2}\Gamma$: total cavity decay rate ($\Gamma = (\kappa_{\mathbf{0}}+\mathbf{2}\kappa_{\mathbf{1}})/\mathbf{2}$)

$\hat{\sigma}_-$: descending operator

$\hat{\sigma}_+$: ascending operator

$\dot{\gamma}$: total decay rate

$\dot{\hat{\sigma}}'$: vacuum noise operator

$\mathbf{w_r}$: transition frequency

$\mathbf{w_c}$: resonant frequency

$|\mathbf{e}\rangle$: excited state of QD

$|\mathbf{g}\rangle$: ground state of QD

$\hat{c}$: basonic annihilation operator of the cavity

g: coupling strength

Input and output relations are shown as [20,23]:

$$\hat{a}_{\mathbf{out}} = \hat{b}_{\mathbf{in}} - \sqrt{\kappa_{\mathbf{1}}}\hat{c} \tag{A.1}$$

$$\hat{b}_{\mathbf{out}} = \hat{a}_{\mathbf{in}} - \sqrt{\kappa_{\mathbf{1}}}\hat{c} \tag{A.2}$$

The motion equations:

$$\frac{\mathbf{d}\hat{c}}{\mathbf{dt}} = -\mathbf{i}\left[\hat{c}, \mathrm{H}\right] - \Gamma\hat{c} + \sqrt{\kappa_{\mathbf{1}}}\left(\hat{a}_{\mathbf{in}} + \hat{b}_{\mathbf{in}}\right) \tag{A.3}$$

$$\frac{\mathbf{d}\hat{\sigma}_-}{\mathbf{dt}} = -\mathbf{i}\left[\hat{\sigma}_-, \mathrm{H}\right] - \gamma\hat{\sigma}_- + \sqrt{\dot{\gamma}}\dot{\hat{\sigma}}' \tag{A.4}$$

H is the Hamiltonian operator as the following:

$$\mathbf{H} = \omega_{\mathbf{c}}\hat{c}^{\dagger}\hat{c} + \omega_{\mathbf{r}}\hat{\sigma}_- + \left[\mathbf{g}\hat{\sigma}_-\hat{c} + \mathbf{h.c}\right] \tag{A.5}$$

$$\hat{\sigma}_-|\, e\rangle = |\, g\rangle \text{ and } \hat{\sigma}_+|\, g\rangle = |\, e\rangle$$

We can rewrite the equations as follows:

$$\hat{\sigma}_- = |\, g\rangle\langle e| \text{ and } \hat{\sigma}_+ = |\, e\rangle\langle g| \text{ so } \hat{\sigma}_- = \hat{\sigma}_+$$

The Hamiltonian equation is transformed into:

$$\mathbf{H} = \omega_{\mathbf{c}}\hat{c}^{\dagger}\hat{c} + \omega_{\mathbf{r}}\hat{\sigma}_-\hat{\sigma}_+ + \left[\mathbf{g}\hat{\sigma}_+\hat{c} + \mathbf{g}^*\hat{c}^{\dagger}\hat{\sigma}_-\right] \tag{A.6}$$

If the motion equations are solved regarding the weak excitation limits, the transport relations in the frequency domain becomes as follows:

If $\hat{c}\,(\omega)$ is solved as:

$$\hat{c}\,(\omega) = \frac{\sqrt{\kappa_{\mathbf{1}}}\left(\hat{a}_{\mathbf{in}}\,(\omega) + \hat{b}_{\mathbf{in}}\,(\omega)\right)}{-\mathbf{i}\,(\omega - \omega_{\mathbf{c}}) + \Gamma - \frac{|\mathbf{g_1}|^{\mathbf{2}}}{\mathbf{i}(\omega - \omega_{\mathbf{r1}}) - \gamma}} \tag{A.7}$$

The input-output relations are:

$$\hat{a}_{\mathbf{out}}(\omega) = \hat{b}_{\mathbf{in}}(\omega) - \frac{\kappa_{\mathbf{1}}\left(\hat{a}_{\mathbf{in}}(\omega) + \hat{b}_{\mathbf{in}}(\omega)\right)}{-\mathbf{i}(\omega - \omega_{\mathbf{c}}) + \Gamma - \frac{|\mathbf{g_1}|^{\mathbf{2}}}{\mathbf{i}(\omega - \omega_{\mathbf{r1}}) - \gamma}} \tag{A.8}$$

$$\hat{b}_{\mathbf{out}}(\omega) = \hat{a}_{\mathbf{in}}(\omega) - \frac{\kappa_{\mathbf{1}}\left(\hat{a}_{\mathbf{in}}(\omega) + \hat{b}_{\mathbf{in}}(\omega)\right)}{-\mathbf{i}(\omega - \omega_{\mathbf{c}}) + \Gamma - \frac{|\mathbf{g_1}|^{\mathbf{2}}}{\mathbf{i}(\omega - \omega_{\mathbf{r1}}) - \gamma}} \tag{A.9}$$

The relations are simplified into:

$$\hat{b}_{\mathbf{in}}(\omega) = \left(\frac{\kappa_{\mathbf{1}}}{-\alpha + \Gamma - \kappa_{\mathbf{1}}}\right)\hat{a}_{\mathbf{in}} + \left(\frac{-\alpha + \Gamma}{-\alpha + \Gamma - \kappa_{\mathbf{1}}}\right)\hat{a}_{\mathbf{out}}(\omega) \tag{A.10}$$

$$\hat{b}_{\mathbf{out}}(\omega) = \left(\frac{\alpha - \Gamma + \kappa_{\mathbf{1}}}{\alpha - \Gamma + \kappa_{\mathbf{1}}}\right)\hat{a}_{\mathbf{in}} + \left(\frac{\kappa_{\mathbf{1}}}{\alpha - \Gamma + \kappa_{\mathbf{1}}}\right)\hat{a}_{\mathbf{out}}(\omega) \tag{A.11}$$

where $\alpha = \mathbf{i}(\omega - \omega_{\mathbf{c}}) + \frac{|\mathbf{g}|^{\mathbf{2}}}{\mathbf{i}(\omega - \omega_{\mathbf{r}}) - \gamma}$

If the equations transform into matrix form:

$$\begin{pmatrix} \hat{b}_{\mathbf{in}}(\omega) \\ \hat{b}_{\mathbf{out}}(\omega) \end{pmatrix} = \frac{\mathbf{1}}{\alpha - \Gamma + \kappa_{\mathbf{1}}} \begin{pmatrix} -\kappa_{\mathbf{1}} & \alpha - \Gamma \\ \alpha - \Gamma + 2\kappa_{\mathbf{1}} & -\kappa_{\mathbf{1}} \end{pmatrix} \begin{pmatrix} \hat{a}_{\mathbf{in}}(\omega) \\ \hat{a}_{\mathbf{out}}(\omega) \end{pmatrix} \tag{A.12}$$

where $\alpha = \mathbf{i}(\omega - \omega_{\mathbf{c}}) + \frac{|\mathbf{g}|^{\mathbf{2}}}{\mathbf{i}(\omega - \omega_{\mathbf{r}}) - \gamma}$

Eq. (A.11) gives the single QD embedded into one cavity. Single-QD-embedded double-cavity array and triple cavity array transmission equations can be derived from Eq. (A.11).

Double-cavity configuration for the transmission equation is:

$$\begin{pmatrix} \hat{b}_{\mathbf{in}}(\omega) \\ \hat{b}_{\mathbf{out}}(\omega) \end{pmatrix} = \frac{\mathbf{1}}{\beta_{\mathbf{2}} - \Gamma + \kappa_{\mathbf{2}}} \begin{pmatrix} -\kappa_{\mathbf{2}} & \beta_{\mathbf{2}} - \Gamma \\ \beta_{\mathbf{2}} - \Gamma + 2\kappa_{\mathbf{2}} & \kappa_{\mathbf{2}} \end{pmatrix} \begin{pmatrix} \mathbf{0} & \mathbf{e}^{\mathbf{j}2\pi} \\ \mathbf{e}^{\mathbf{j}2\pi} & \mathbf{0} \end{pmatrix}$$

$$\frac{\mathbf{1}}{\beta_{\mathbf{1}} - \Gamma + \kappa_{\mathbf{1}}} \begin{pmatrix} -\kappa_{\mathbf{1}} & \beta_{\mathbf{1}} - \Gamma \\ \beta_{\mathbf{1}} - \Gamma + \mathbf{2}\kappa_{\mathbf{1}} & \kappa_{\mathbf{1}} \end{pmatrix} \begin{pmatrix} \hat{a}_{\mathbf{in}}(\omega) \\ \hat{a}_{\mathbf{out}}(\omega) \end{pmatrix} \tag{A.13}$$

where

$$\beta_{\mathbf{1}} = \mathbf{i}(\omega - \omega_{\mathbf{c1}}) + \frac{|\mathbf{g_1}|^{\mathbf{2}}}{\mathbf{i}(\omega - \omega_{\mathbf{r1}}) - \gamma}$$

and $\beta_{\mathbf{2}} = \mathbf{i}(\omega - \omega_{\mathbf{c2}})$.

In order to get the transmission equation of triple-cavity configuration, the coupling strength values are accepted as $g_1 = g_2 = g_3 = 0$

$$\begin{pmatrix} \hat{b}_{\mathbf{in}}(\mathbf{w}) \\ \hat{b}_{\mathbf{out}}(\mathbf{w}) \end{pmatrix} = \frac{\mathbf{1}}{\beta_{\mathbf{3}} - \Gamma + \kappa_{\mathbf{3}}} \begin{pmatrix} -\kappa_{\mathbf{3}} & \beta_{\mathbf{3}} - \Gamma \\ \beta_{\mathbf{3}} - \Gamma + 2\kappa_{\mathbf{3}} & \kappa_{\mathbf{3}} \end{pmatrix} \begin{pmatrix} \mathbf{0} & \mathbf{e}^{\mathbf{j}2\pi} \\ \mathbf{e}^{\mathbf{j}2\pi} & \mathbf{0} \end{pmatrix}$$

$$\frac{\mathbf{1}}{\beta_{\mathbf{2}}-\Gamma+\kappa_{\mathbf{2}}}\begin{pmatrix} -\kappa_{\mathbf{2}} & \beta_{\mathbf{2}}-\Gamma \\ \beta_{\mathbf{2}}-\Gamma+2\kappa_{\mathbf{2}} & \kappa_{\mathbf{2}} \end{pmatrix}\begin{pmatrix} \mathbf{0} & \mathbf{e^{j2\pi}} \\ \mathbf{e^{j2\pi}} & \mathbf{0} \end{pmatrix}$$

$$\frac{\mathbf{1}}{\beta_{\mathbf{1}}-\Gamma+\kappa_{\mathbf{1}}}\begin{pmatrix} -\kappa_{\mathbf{1}} & \beta_{\mathbf{1}}-\Gamma \\ \beta_{\mathbf{1}}-\Gamma+2\kappa_{\mathbf{1}} & \kappa_{\mathbf{1}} \end{pmatrix}\begin{pmatrix} \hat{a}_{\mathbf{in}}(\mathbf{w}) \\ \hat{a}_{\mathbf{out}}(\mathbf{w}) \end{pmatrix} \tag{A.14}$$

where $\beta_j = i(\omega - \omega_{cj})$.

Eqs. (A.14) and (A.15) solved, and then transmission $(\hat{b}_{out}(w)/\hat{a}_{in}(w))$ equations are shown as:

$$\mathbf{t}(\omega) = \frac{\left(\mathbf{2}\omega^{\mathbf{2}}\kappa_{\mathbf{0}} - \frac{\mathbf{1}}{\mathbf{2}}\mathbf{g}^{\mathbf{2}}\kappa_{\mathbf{0}} - \frac{\mathbf{1}}{\mathbf{4}}\kappa_{\mathbf{0}}^{\mathbf{3}}\right) + \mathbf{i}\omega\left(-\omega^{\mathbf{2}} + \mathbf{g}^{\mathbf{2}} + \frac{\mathbf{5}}{\mathbf{4}}\kappa_{\mathbf{0}}^{\mathbf{2}}\right)}{\left(\mathbf{2}\omega^{\mathbf{2}}\kappa_{\mathbf{0}} + \mathbf{2}\kappa\omega^{\mathbf{2}} - \kappa\mathbf{g}^{\mathbf{2}} - \frac{\mathbf{1}}{\mathbf{2}}\mathbf{g}^{\mathbf{2}}\kappa_{\mathbf{0}} - \kappa_{\mathbf{0}}^{\mathbf{2}}(\kappa + \frac{\mathbf{1}}{\mathbf{4}}\kappa_{\mathbf{0}})\right) + \mathbf{i}\omega\left(\mathbf{g}^{\mathbf{2}} - \omega^{\mathbf{2}} + \mathbf{3}\kappa\kappa_{\mathbf{0}} + \frac{\mathbf{5}}{\mathbf{4}}\kappa_{\mathbf{0}}^{\mathbf{2}}\right)} \tag{A.15}$$

$$\mathbf{t}(\omega) = \frac{\left(\frac{\mathbf{3}}{\mathbf{2}}\omega^{\mathbf{2}}\kappa_{\mathbf{0}} - \frac{\mathbf{1}}{\mathbf{8}}\kappa_{\mathbf{0}}^{\mathbf{3}} - \frac{\mathbf{1}}{\mathbf{2}}\kappa_{\mathbf{0}}\,\omega^{\mathbf{2}}\right) + \mathbf{i}\omega\left(-\omega^{\mathbf{2}} + \frac{\mathbf{3}}{\mathbf{4}}\kappa_{\mathbf{0}}^{\mathbf{2}} + \omega^{\mathbf{2}}\right)}{\left(\mathbf{3}\omega^{\mathbf{2}}\kappa + \frac{\mathbf{3}}{\mathbf{2}}\omega^{\mathbf{2}}\kappa_{\mathbf{0}} - \frac{\mathbf{3}}{\mathbf{4}}\kappa\kappa_{\mathbf{0}}^{\mathbf{2}} - \frac{\mathbf{1}}{\mathbf{8}}\kappa_{\mathbf{0}}^{\mathbf{3}} - \omega^{\mathbf{2}}(\kappa + \frac{\mathbf{1}}{\mathbf{2}}\kappa_{\mathbf{0}})\right) + \mathbf{i}\omega\left(\omega^{\mathbf{2}} - \omega^{\mathbf{2}} + \mathbf{3}\kappa\kappa_{\mathbf{0}} + \frac{\mathbf{3}}{\mathbf{4}}\kappa_{\mathbf{0}}^{\mathbf{2}}\right)} \tag{A.16}$$

when $\gg \kappa_{\mathbf{0}}$:

$$\mathbf{t}(\omega) = \frac{\left(\mathbf{2}\omega^{\mathbf{2}}\kappa_{\mathbf{0}} - \frac{\mathbf{1}}{\mathbf{2}}\mathbf{g}^{\mathbf{2}}\kappa_{\mathbf{0}}\right) + \mathbf{i}\omega\left(-\omega^{\mathbf{2}} + \mathbf{g}^{\mathbf{2}}\right)}{\left(\mathbf{2}\kappa\omega^{\mathbf{2}} - \kappa\mathbf{g}^{\mathbf{2}}\right) + \mathbf{i}\omega\left(\mathbf{g}^{\mathbf{2}} - \omega^{\mathbf{2}} + \mathbf{3}\kappa\kappa_{\mathbf{0}}\right)} \tag{A.17}$$

$$\mathbf{t}(\omega) = \frac{\left(\frac{\mathbf{3}}{\mathbf{2}}\omega^{\mathbf{2}}\kappa_{\mathbf{0}} - \frac{\mathbf{1}}{\mathbf{8}}\kappa_{\mathbf{0}}^{\mathbf{3}}\right) + \mathbf{i}\omega\left(-\omega^{\mathbf{2}} + \mathbf{g}^{\mathbf{2}}\right)}{\left(\mathbf{3}\omega^{\mathbf{2}}\kappa - \omega^{\mathbf{2}}\kappa\right) + \mathbf{i}\omega\left(\omega^{\mathbf{2}} - \omega^{\mathbf{2}} + \mathbf{3}\kappa\kappa_{\mathbf{0}}\right)} \tag{A.18}$$